Supporting Information

4–Amino–1–(3–mercapto–propyl)–pyridine hexafluorophosphate ionic liquid functionalized gold nanoparticles for IgG immunosensing enhancement

Rui Li[†], Changxian Liu[†], Kangbing Wu[‡], Yin Huang[†], Yanying Wang[†], Huaifang Fang[†], Huijuan Zhang[†], Chunya Li [*,†]

[†] Key Laboratory of Analytical Chemistry of the Satate Ethnic Affairs Commission, College of Chemistry and Materials Science, South–Central University for Nationalities, Wuhan 430074, China

[‡]Key Laboratory for Large-Format Battery Materials and System, Ministry of Education, School of Chemistry and Chemical Engineering, Huazhong University of Science and Technology, Wuhan 430074, China

* Corresponding author. E-mail: lichychem@163.com.

Table of content

Figure S6 The oxidation peak current of 5.0×10^{-3} mol L^{-1} $K_3Fe(CN)_6/K_4Fe(CN)_6$ at the immunosensor, which was blocked with BSA, before (a) and after being interacted with 50.0 ng mL^{-1} human IgG (b), AFP (c) and PSA (d);

The oxidation peak current of 5.0×10^{-3} mol L^{-1} $K_3Fe(CN)_6/K_4Fe(CN)_6$ at the immunosensor, which was not blocked with BSA, before (a') and after being interacted with 50.0 ng mL^{-1} human IgG (b'), AFP (c') and PSA (d');

Table S1 Comparison of analytical characteristics of the human IgG immunosensor with previous reports.

Table S2 Analytical characteristics of some commercial kits for human IgG.

Table S3 Influence of potential interferences on the current response of immunosensor (n=5).

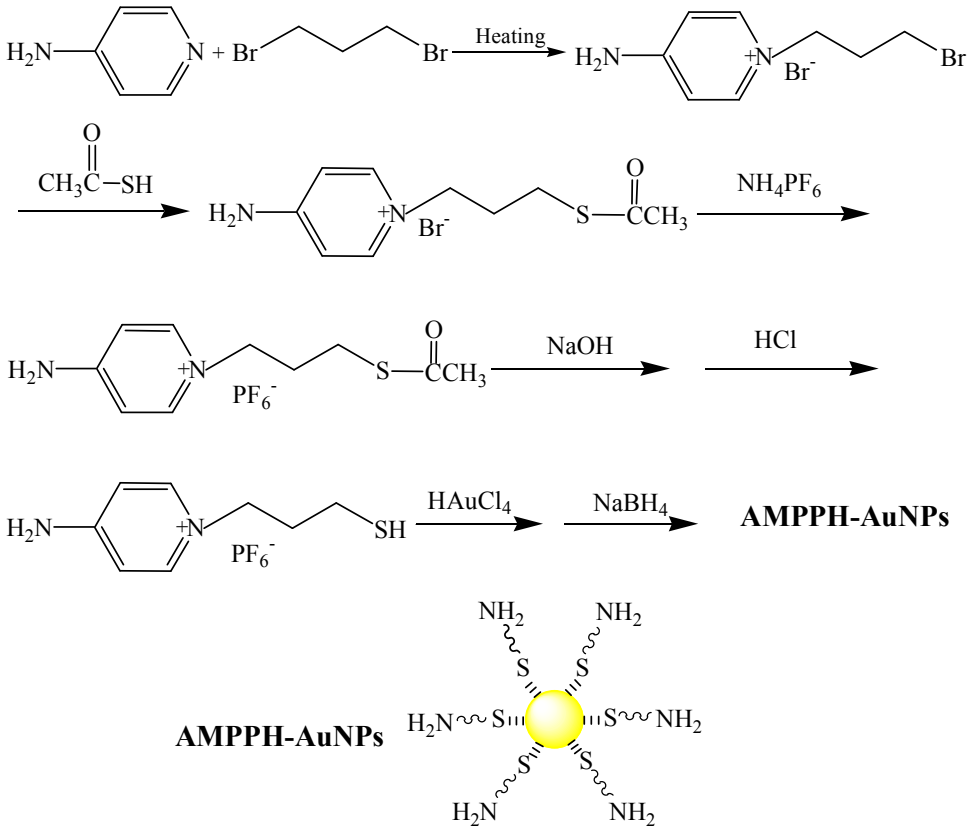

Scheme S1 Schematic illumination for the synthesis of AMPPH ionic liquid and AMPPH-AuNPs.

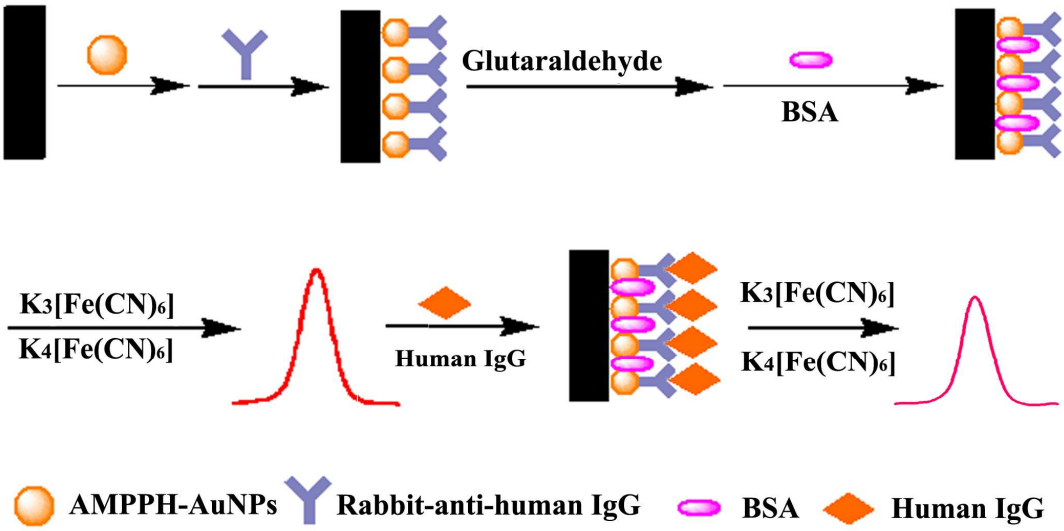

Scheme S2 Schematic illustration of the IgG immunosensing system.

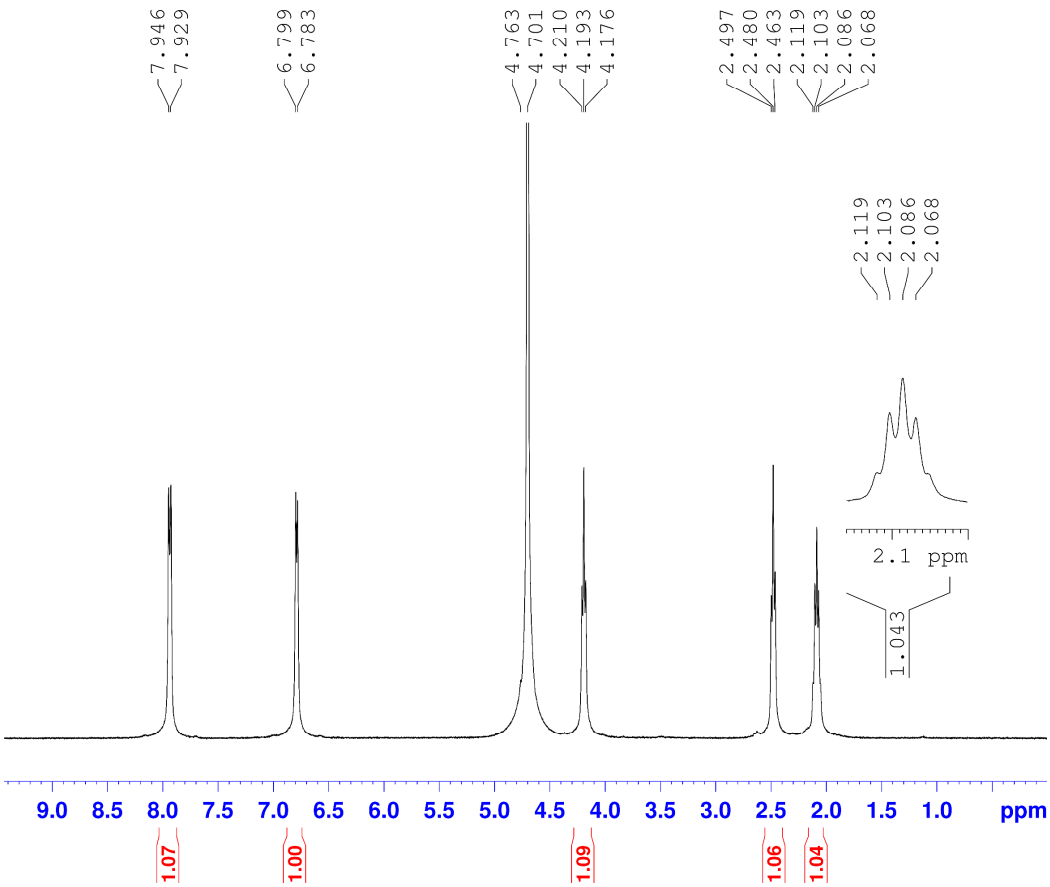

Figure S1 ^{1}H-NMR spectrum of 4–amino–1–(3–mercapto–propyl)–pyridine hexafluorophosphate ionic liquid (solvent: D_2O).

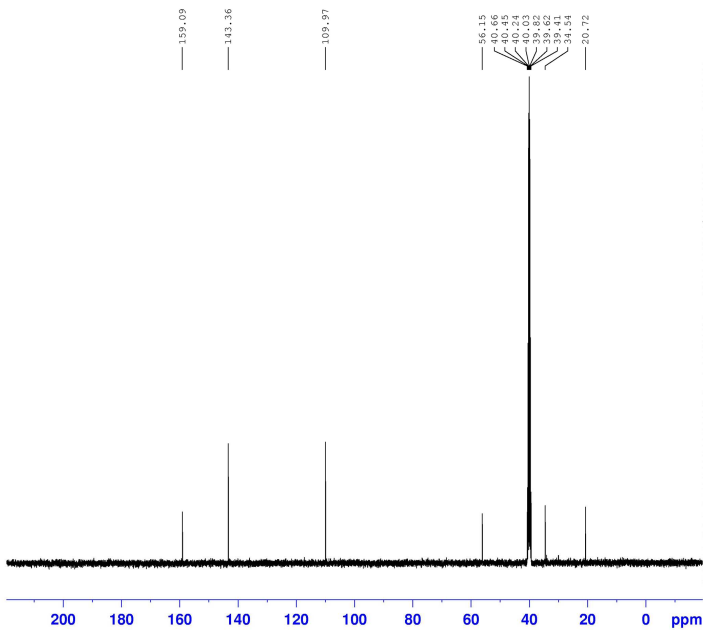

Figure S2 ^{13}C-NMR spectrum of 4–amino–1–(3–mercapto–propyl)–pyridine hexafluorophosphate ionic liquid (solvent: DMSO).

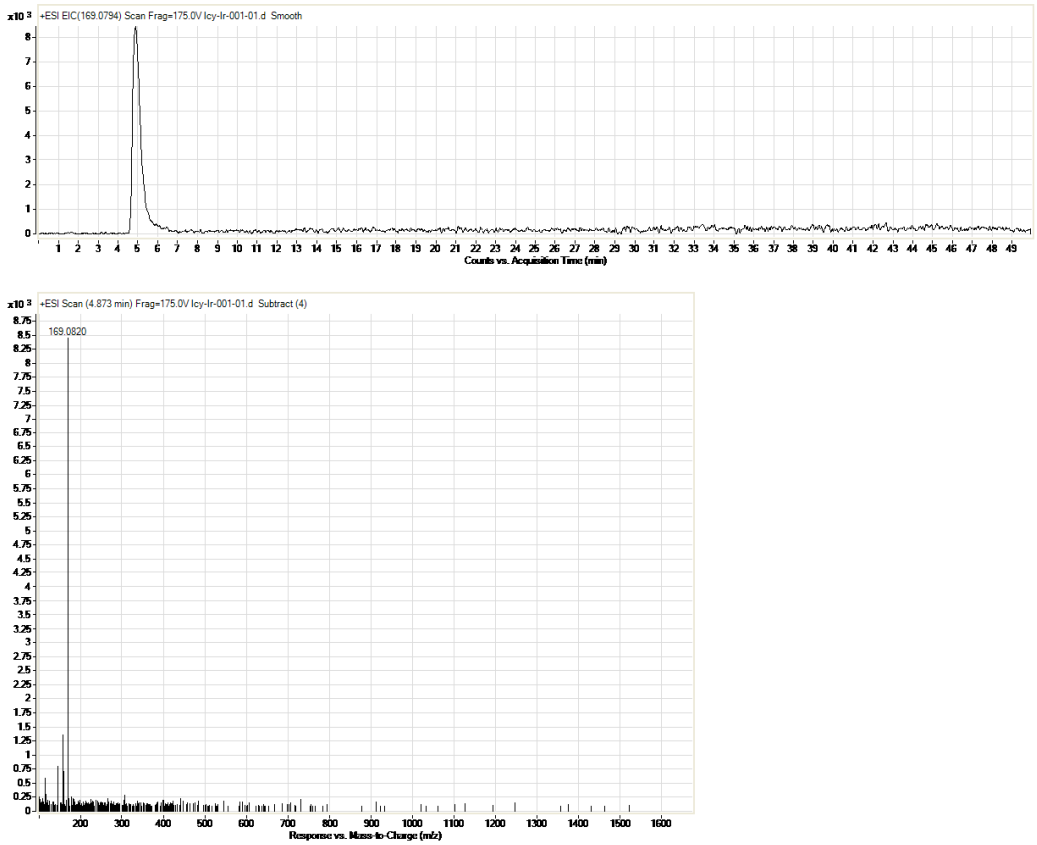

Figure S3 HPLC-Mass spectrum of 4–amino–1–(3–mercapto–propyl)–pyridine hexafluorophosphate ionic liquid.

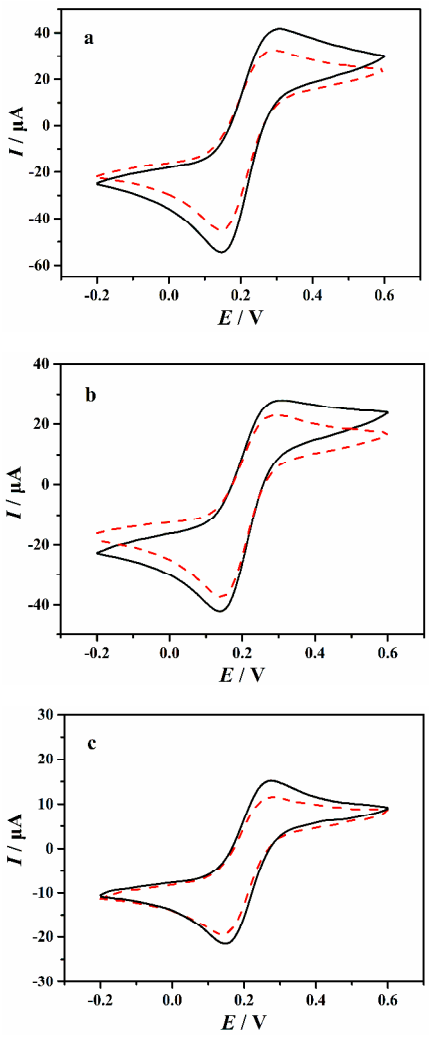

Figure S4 Cyclic voltammograms of 5.0×10^{-3} mol L^{-1} $K_3Fe(CN)_6/K_4Fe(CN)_6$ at the immunosensors, which were respectively fabricated with AMPPH-AuNPs (a), AuNPs (b) and AMPPH ionic liquid (c), before (black solid line) and after (red dash line) being interacted with 50.0 ng mL^{-1} human IgG.

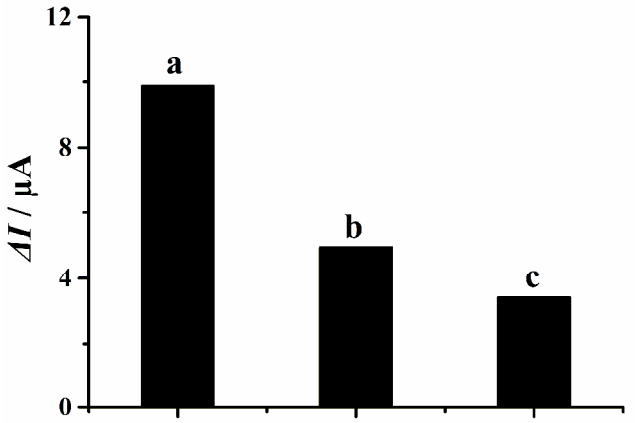

Figure S5 The oxidation peak current difference of 5.0×10^{-3} mol L^{-1} $K_3Fe(CN)_6/K_4Fe(CN)_6$ at the immunosensors, which were respectively fabricated with AMPPH-AuNPs (a), AuNPs (b) and AMPPH ionic liquid (c), before and after being interacted with 50.0 ng mL^{-1} human IgG.

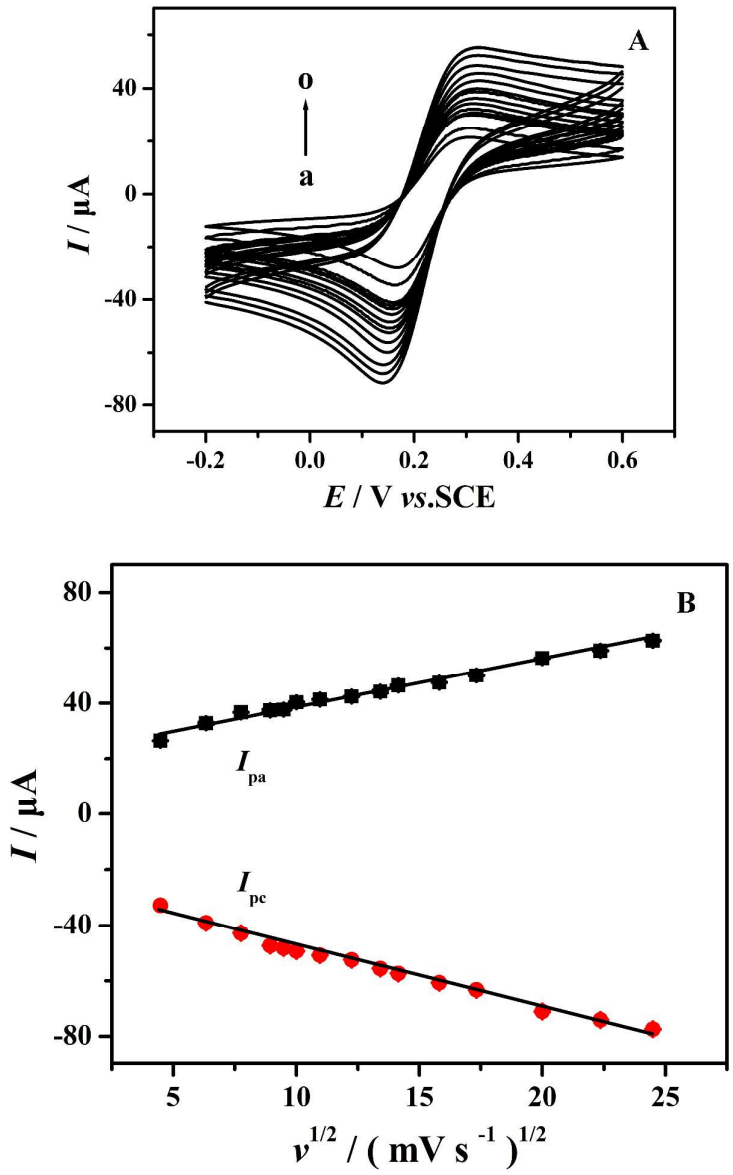

Figure S6 (A) Cyclic voltammograms of immunosensing system in 5.0×10^{-3} mol L^{-1} $K_3Fe(CN)_6/K_4Fe(CN)_6$ solution at scan rate of 0.02, 0.04, 0.06, 0.08, 0.09, 0.1, 0.12, 0.15, 0.18, 0.2, 0.25, 0.3, 0.4, 0.5 and 0.6 V s^{-1} (From curve a to o); (B) The relationship between the current response and the square root of scan rate.

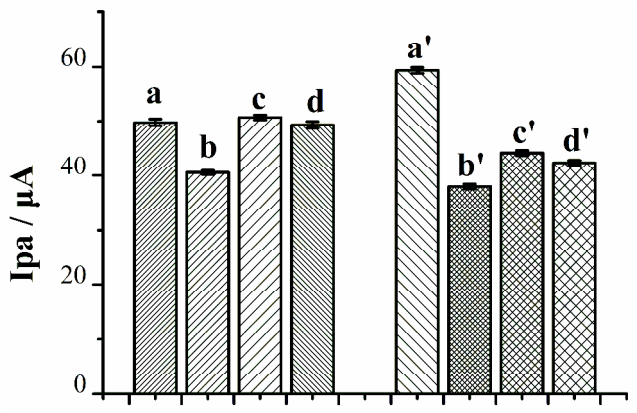

Figure S 7 The oxidation peak current of 5.0×10^{-3} mol L^{-1} $K_3Fe(CN)_6/K_4Fe(CN)_6$ at the immunosensor, which was blocked with BSA, before (a) and after being interacted with 50.0 ng mL^{-1} human IgG (b), AFP (c) and PSA (d);

The oxidation peak current of 5.0×10^{-3} mol L^{-1} $K_3Fe(CN)_6/K_4Fe(CN)_6$ at the immunosensor, which was not blocked with BSA, before (a') and after being interacted with 50.0 ng mL^{-1} human IgG (b'), AFP (c') and PSA (d');

Table S1 Comparison of analytical characteristics of the IgG immunosensor with previous reports.

Method	Materials	Linear range (ng mL^{-1})	Detection limit (ng mL^{-1})	Ref.
Votammetric immunosensor	4–amino–1–(3–mercapto–propyl)–pyridine hexafluorophosphate modified gold nanoparticles	0.1 – 100	0.08	This method
Amperometric immunosensor	iridium oxide matrices	10 – 200	8	1
Sandwich-type amperometric immunosensor	SiO_2 nanoparticle	1.5 – 2250	0.75	2
Amperometric immunosensor	Multifunctional mesoporous silica nanoparticles	0.01 – 10	-	3
Sandwich-type amperometric immunosensor	Carbon Sphere/Gold Nanoparticle	0.10 – 10	0.09	4
Sandwich-type voltammetric immunosensor	gold nanoparticles decorated graphene nanosheets and palladium nanoparticle decorated carbon nanotube	0.50 – 10	0.44	5
Sandwich-type voltammetric immunosensor	Layer-by-layer assembly of chemical reduced graphene and carbon nanotubes	1.0 – 500	0.2	6
Sandwich-type voltammetric immunosensor	poly(m-aminophenol) modified expanded graphite electrode	5000 – 60000	190	7
Potentiometric immunosensor	Fe_3O_4 Nanoparticles	0.1 – 1.2	0.023	8
Amperometric immunosensor	Conducting polymer and carbon nanotube-linked hydrazine	0.1 – 10	0.084+0.004	9
Voltammetric immunosensor	COOH–multiwalled carbon nanotubes/Fe_3O_4	30 – 1000	25	10
Electrochemiluminescence	electrochemically reduced graphene oxide and gold nanoparticles	0.02 – 100	0.013	11
Amperometric immunosensor	ZnO/chitosan composite	2.5 – 500	1.2	12
Amperometric immunosensor	$CdFe_2O_4$ magnetic nanoparticles	510 – 30170	180	13
Electrochemiluminescence	Thiolacetic acid self-assembled monolayers on AuSb alloy electrode	1.0 – 1000	0.3	14

References

(1) Wilson, M.S.; Rauh, R.D. *Biosens. Bioelectron.* **2004**, 19, 693–699.

(2) Zhong, Z.Y.; Li, M.X.; Xiang, D.B.; Dai, N.; Qing, Y.; Wang, D.; Tang, D.P. *Biosens. Bioelectron.* **2009**, 24, 2246–2249.

(3) Yang, M.H.; Li, H.; Javadi, A.; Gong, S.Q. *Biomater.* **2010**, 31, 3281–3286.

(4) Xu, Q.N.; Yan, F.; Lei, J.P.; Leng, C.; Ju, H.X. *Chem. Eur. J.* **2012**, 18, 4994 – 4998.

(5) Leng, C.; Wu, J.; Xu, Q.N.; Lai, G.S.; Ju, H.X.; Yan, F. *Biosens. Bioelectron.* **2011**, 27, 71– 76.

(6) Liu, Y.; Liu, Y.; Feng, H.B.; Wu, Y.M.; Joshi, L.; Zeng, X.Q.; Li, J.H. *Biosens. Bioelectron.* **2012**, 35, 63– 68.

(7) Tao,Y.X.; Liu, Q.X.; Li, W.; Xue, H.G.; Qin, Y.; Ge, J.F.; Kong, Y. *Synthetic Met.* **2013**, 183, 50– 56

(8) Li, J.P.; Gao, H.L. *Electroanal.* **2008**, 20, 881–887.

(9) Zhu, Y.; Choon W.; Koh, A.; Shim, Y.B. *Electroanal.* **2010**, 22, 2908–2914.

(10) Zarei, H.; Ghourchian, H.; Eskandari, K.; Zeinali, M. *Anal. Biochem.* **2012**, 421, 446–453.

(11)Peng, S.S.; Zou, G.Z.; Zhang, X.L.; *J. Electroanal. Chem.* **2012**, 686, 25–31.

(12) Wang, Z.J.; Yang, Y.H.; Li, J.S.; Gong, J.L.; Shen, G.L.; Yu, R.Q. *Talanta* **2006**, 69, 686–690.

(13) Liu, Z.M.; Yang, H.F.; Li, Y.F.; Liu, Y.L.; Shen, G.L.; Yu, R.Q. *Sensor. Actuat. B*, **2006**,113, 956–962.

(14) Wu, A.H.; Sun, J.J.; Fang, Y.M.; Su, X.L.; Chen, G.N. *Talanta* **2010**, 82, 1455–1461.

Table S2 Analytical characteristics of some commercial kits for human IgG.

Dynamic range (ng mL^{-1})	Detection limit (ng mL^{-1})	Sensitivity (ng mL^{-1})	Web site
0.1 – 100	0.08	-	This method
1.6 – 100	1.6	1.6	http://www.ebioscience.com/human-ig-g-total-ready-set-go-elisa-kit.htm
0.24 – 1000	0.24	-	http://www.perkinelmer.com.cn/Catalog/Family/ID/AlphaLISA+Human+IGg+Research+Immunoassay+Kits
0.69 – 500	-	-	http://www.funakoshi.co.jp/data/datasheet/BET/E88-104.pdf
10 – 640	-	10	http://www.clontech.com/takara/US/Products/Cell_Biology/Miscellaneous/Reagents_Kits/IgG-Human_EIA_Kit
0.2 – 100	-	-	https://www.mabtech.com/sites/default/files/datasheets/3850-1AD-6.pdf
0.021 – 15	-	< 0.15	http://www.abcam.cn/igg-human-elisa-kit-ab100547.html
1.25 – 80.0	1.2	-	http://www.abnova.com/products/products_detail.asp?Catalog_id=KA3817

Table S3 Influence of potential interferences on the current response (n=5).

Antigens	Oxidation peak current (μA)					Average (μA)	RSD (%)
IgG	39.78	39.26	39.41	41.53	39.69	39.93	2.3
IgG-PSA	40.21	41.32	39.04	40.36	40.85	40.36	2.1
IgG-AFP	41.56	39.47	41.88	40.75	39.04	40.54	3.1